energies

MDPI

Article

A Comparative Study of Laminar-Turbulent Displacement in anEccentric Annulus Under Imposed Flow Rate and Imposed Pressure Drop Conditions

Yasaman Foolad [1,‡], Majid Bizhani [1,‡] and Ian A. Frigaard [2,*,†]

[1] Department of Mechanical Engineering, University of British Columbia, Vancouver, BC V6T 1Z4, Canada; yasamanfoolad@gmail.com (Y.F.); bizhani@ualberta.ca (M.B.)
[2] Departments of Mathematics and Mechanical Engineering, University of British Columbia, Vancouver, BC V6T 1Z4, Canada
* Correspondence: frigaard@mail.ubc.ca
† Current address: 1984 Mathematics Road, Vancouver, BC V6T 1Z2, Canada.
‡ These authors contributed equally to this work.

Abstract: This paper presents a series of experiments focused on the displacement of viscoplastic fluids by various Newtonian and non-Newtonian fluids from a long horizontal, eccentric annulus. The flow regimes range from high Reynolds number laminar regimes through to fully turbulent. These experiments represent the primary cementing operation in a horizontal well. The main objective of our experiments is to gain insight into the role of the flow regime in the fluid-fluid displacement flows of relevance to primary cementing. We study strongly eccentric annuli and displaced fluids with a significant yield stress, i.e., those scenarios where a mud channel is most likely to persist. For fully eccentric annuli, the displacements are uniformly poor, regardless of regime. This improves for an eccentricity of 0.7. However, at these large eccentricities that are typical of horizontal well cementing, the displacement is generally poor and involves a rapid "breakthrough" advance along the wide upper side of the annulus followed only by a much slower removal of the residual fluids. This dynamic renders contact time estimates meaningless. We conclude that some of the simple statements/preferences widely employed in industry do not necessarily apply for all design scenarios. Instead, a detailed study of the fluids involved and the specification of the operational constraints is needed to yield improved displacement quality.

Keywords: annular flow; primary cementing; turbulence; imposed flow rate; imposed pressure drop

Citation: Foolad, Y.; Bizhani, M.; Frigaard, I.A. A Comparative Study of Laminar-Turbulent Displacement in anEccentric Annulus Under Imposed Flow Rate and Imposed Pressure Drop Conditions. *Energies* **2021**, *14*, 1654. https://doi.org/10.3390/en14061654

Academic Editor: Victor Terekhov

Received: 3 February 2021
Accepted: 8 March 2021
Published: 16 March 2021

1. Introduction

Every well undergoes primary cementing at least once during construction and potentially many times, according to the well complexity. In this operation, after the casing/liner is placed into the borehole, a sequence of fluids is circulated down inside the casing/liner and upwards in the surrounding annulus. The average annular gap is typically 2–3 cm, and the drilling fluid/mud that is initially in the well can be difficult to remove due to its rheology. In particular, the yield stress of the mud, which is important in suspending cuttings during drilling, makes the mud harder to remove from the walls and narrow side of the annulus. Residual mud affects the hydraulic bond of the cement to the casing and formation, contributing to well leakage. The many negative consequences of leakage include reduced well productivity [1], contamination of potable groundwater, ecological damage (oil surface leaks), greenhouse gas emissions (CH_4), and safety risks (H_2S). It is also technically challenging to repair a cemented well through remedial cementing, with low success rates. These factors have increased interest in the primary cementing operation.

Typically, a low viscosity low density Newtonian wash starts the sequence, followed by a denser and more viscous spacer fluid. Finally, the cement slurry is pumped, which may consist of a lead and tail slurry. In terms of hydraulic design, the choices of fluids and flow

rates in primary cementing are flexible provided that the annular pressures lie within the pore-fracenvelope during placement. Material and mechanical goals strongly influence the cement properties, and (except for high cost wells) the drilling muds will not be replaced prior to cementing. Thus, to some extent, design optimization focuses on wash/spacer properties constrained by density and flow rate limits. This is the area we examine in this paper.

Over the past 50 years, the preferred method for mud removal during cementing has been to pump the fluids in a fully turbulent regime. This is widely believed to be the more effective means of removing drilling mud [2–4] and is included in many industry recommended practices, e.g., [5]. As wells have become deeper and have included long horizontal sections, pressure constraints on pumping have become tighter. It is thus less common to be able to pump all fluids in a fully turbulent regime, especially the more viscous spacers and cement slurries. Therefore, it becomes necessary to consider designs with varied flow regimes and to study how operational constraints such as fixed flow rates or fixed pressure drops affect displacement efficiency.

Recent studies have also questioned the validity of this widely accepted perception that turbulent displacement is necessarily superior to laminar displacement, e.g., warning that certain conditions must be met for turbulent displacement to succeed [1,6]. Various aspects of this matter were examined in the work of Maleki and Frigaard [7], Kelessidis et al. [3], Enayatpour and van Oort [8], and Lavrov and Torsæter [2]. Three key concerns are: (i) the generality of these statements, instead of addressing specific scenarios; (ii) the lack of objective comparisons between methods; (iii) the fact that it is rare in modern wells to be able to pump all fluids in a turbulent regime.

For example, in the studies performed by Smith and Ravi [9] and Howard and Clark [10], it was illustrated that displacement efficiency was improved in displacement experiments with higher flow rates, but they did not compare laminar and turbulent regimes despite being often cited in this regard. Similarly, the studies by Haut and Crook [11] and Smith [12] suggest that "high flow rates, whether or not the cement is in turbulent, provide better displacement than plug flow rates" and "as the annular velocity is increased there is no sharp increase in the displacement efficiency at the transition from laminar to turbulent flow". Thus, it is necessary to study specific scenarios of turbulent flow and where laminar-turbulent comparisons can be made.

In a typical design, the purpose of the Newtonian wash is to promote turbulence around the entire circumference of the annulus, and as part of the design, a 10 min contact time is frequently recommended [13]. In vertical wells however, the combination of the low density and viscosity of the wash with the eccentricity of the well leads to the rapid progression of the wash along the wide side of the annulus [14]. Thus, the problematic narrower parts of the annulus see little effect of the wash, and the contact time estimates are no longer valid. Studies such as [14,15] make questionable the effectiveness of turbulent washes and whether they should be a part of industry recommended practice. Here, we will explore this aspect further experimentally in a horizontal geometry, where density effects are reduced [16] and where the annulus is generally more eccentric.

Maleki and Frigaard [15] studied turbulent cementing in detail, using both scaling arguments and model simulations. First, it was shown that rheology becomes insignificant for a fully turbulent displacement flow. The authors performed a set of displacement simulations where the displacing fluid rheology varied, but the nominal effective viscosity was constant. The results showed no discernible difference. However, if either fluid becomes laminar (even partially), then the rheology becomes relevant. Secondly, it was shown that even if turbulence aids displacement, further increases in the flow rate can negate these benefits, i.e., one can be too turbulent. In particular, in a vertical well, a positive density difference can be shown to help stabilize the interface [15], which counters the adverse impact of casing eccentricity and promotes an even displacement all around the annulus. However, for high flow rates, the turbulent stresses ($-\rho\overline{u'v'} \approx \frac{1}{2} f \rho U^2$) become much larger than the buoyancy stresses ($\Delta\rho g D$). Buoyancy becomes irrelevant to the

displacement, and only the underlying eccentricity of the annulus remains to influence the flow: the displacement front advances faster up the wide side of the annulus. In a second study [17], the authors compared laminar and turbulent cementing under a fixed frictional pressure drop constraint. A new metric for quantifying displacement performance was introduced in which instead of using the volumetric efficiency of the whole annulus, only the volumetric efficiency of the narrow side was used. The first criterion is commonly used in industry, but is dominated by the wide side displacement and is not sensitive to displacement defects, which typically occur on the narrow side. The study showed that turbulence is not necessarily superior to laminar displacement, as long as the same operational constraints are applied.

Here, we re-examine the wash/spacer-mud system from an experimental perspective, using analogue fluids in a laboratory flow loop. One aspect of turbulent flow that is not considered in the 2D model of Maleki and Frigaard [18] is the development of secondary flows and what influence they may have on the removal of gelled fluid. Secondary flows are typically only 1–2% of the streamwise velocity [19]. However, there are instances involving viscoplastic fluids where the stress field is not approximated to leading order only by the shear flow terms, e.g., the eccentric annular flow of Walton and Bittleston [20]. In this and similar flows with slow streamwise variation, the unyielded plug regions also contain significant normal stresses, which means that yielding/removal by secondary flows may be more effective than expected. Secondary flows in eccentric annuli have been studied to some depth [21,22] and show the appearance of two counter-rotating vortices on each side of the plane of symmetry, which transfer high velocity fluid from the wide gap to the narrow gap and return low momentum fluid. In the displacement context, our recent study [23] suggested that these secondary flows do indeed positively affect the displacement of unyielded fluid on the narrow side of strongly eccentric annuli.

Our study is targeted at the displacement of viscoplastic fluids in highly eccentric annuli by low viscous fluids in various flow regimes. Specifically, we look into the following questions: (i) At a fixed flow rate, what are the effects of flow regime on displacement efficiency? (ii) At a fixed pump capacity (pressure drop), how does a turbulent displacement compare with a laminar displacement? Does the intensity of turbulence (i.e., weak or strong turbulence) affect the outcome?

2. Materials and Methods

Given the difficulties of direct field observation and measurement, we studied the displacement flows in a horizontal, eccentric annulus in a lab-scale experiment, which allowed visualization.

2.1. Horizontal Flow Loop

A schematic of the experimental setup is presented in Figure 1. The flow loop is designed to simulate the displacement of one fluid with another. The system is built such that the displacing fluid and the displaced fluid are flowing simultaneously at the same flow rate prior to the displacement, to minimize acceleration effects. Initially, Fluid 1 (displaced fluid) is flowing through the test section, while Fluid 2 (displacing fluid) is diverted through a bypass line. Upon activating the two pneumatic valves simultaneously, Fluid 2 is diverted to the test section, while Fluid 1 changes direction to a bypass line.

The test section has a total length of 7.5 m made of optic-grade borosilicate glass pipes, each 1.5 m long with an inner diameter of 52 mm. The inner body is a stainless steel pipe with an outer diameter of 38 mm. The annulus has a radius ratio of 0.73 and a hydraulic diameter of 14 mm. To minimize the sagging and vibration of the internal pipe, the inner pipe wall thickness was selected to be 1.25 mm, satisfying near neutral buoyancy in a water based solution, e.g., as [24]. To fix and control the eccentricity, a 3 mm rod was used every 1.5 m of the test section, which passed through the internal steel pipe and was fixed to it. Table 1 summarizes the relevant dimensions of the flow loop. For the eccentricity e,

the distance Δy_c is the vertical distance between the centers of the inner and outer pipes, measured downwards.

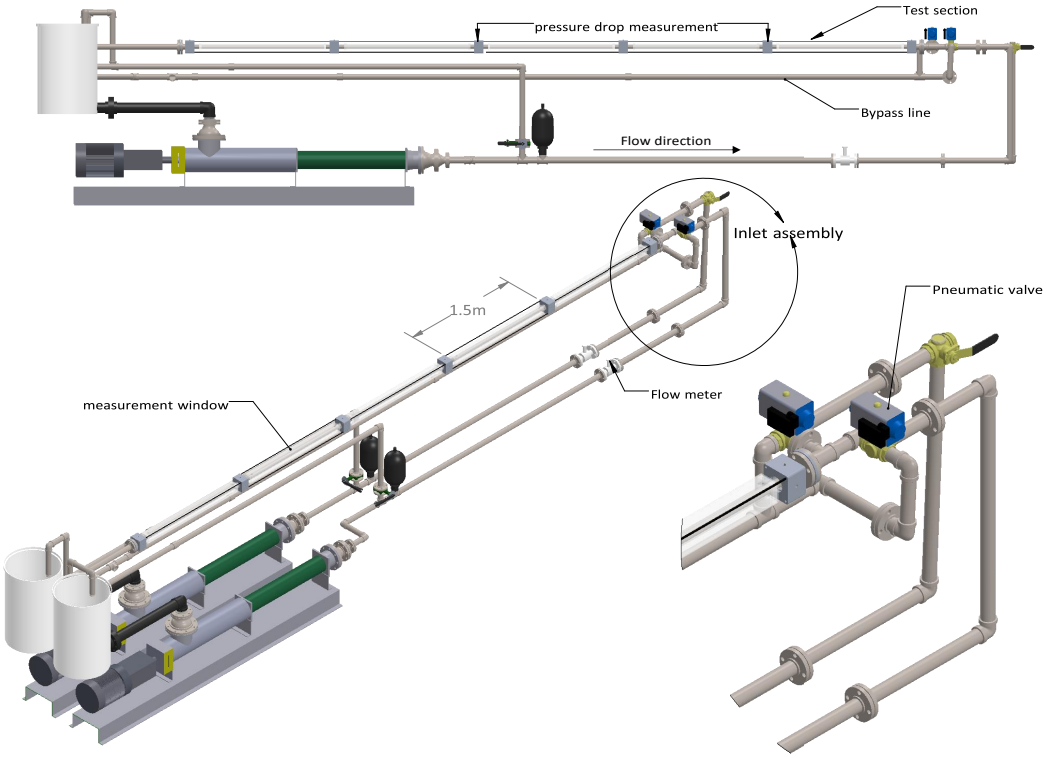

Figure 1. Schematic of the flow loop.

Table 1. Dimensions of the flow loop.

Description	Definition	Dimension
Outer pipe radius	R_o	26 mm
Inner pipe radius	R_i	19 mm
Aspect ratio	$\frac{\delta}{\pi} = \frac{1}{\pi}\frac{R_o - R_i}{R_o + R_i}$	0.05
Radius ratio	$\alpha = \frac{R_i}{R_o}$	0.73
Hydraulic diameter	$D_h = 2(R_o - R_i)$	14 mm
Eccentricity	$e = \frac{\Delta y_c}{R_o - R_i}$	0 to 1
Axial length	$\xi = \frac{L}{\frac{\pi}{2}(R_o + R_i)}$	106

The fluids were circulated through the loop using two progressive cavity pumps (PCPs) equipped with variable frequency drives (VFDs). The flow rates were measured using a set of two magnetic flow meters (OMEGA FMG 606-R) with an accuracy of ±0.5%, each incorporated at the inlet of the test section and the bypass line. The temperature of each fluid was monitored and recorded by two thermocouples mounted in the tanks. The pressure drop along the annular test section was determined using a high accuracy, differential pressure transducer (OMEGA DPG 409-050DWU) acting over a 3.0 m distance. The pressure transducer had a measurement range of 0–50 psi and an accuracy of 0.08%, and its probes were located at an adequate distance downstream of the inlet ($>88D_H$). Regulating pump speeds, controlling pneumatic actuated valves, and collecting all data such as flow rates, pressure drop, and temperatures were managed by a computerized data acquisition system equipped with the LabView software developed by National Instruments.

2.2. Measurement Methodology

Direct visualization of the fluid-fluid interaction is the primary measurement technique we used. To minimize visualization errors (i.e., magnification) caused by the cylindrical shape of the pipes, the glass pipes were put inside rectangular Plexiglas boxes filled with glycerol, with a refractive index similar to that of borosilicate glass, to reduce light refraction. The displacing fluid was dyed using red fluorescent dye (excitation wavelength of 600 nm) and the displaced fluid dyed using black ink, to produce a high contrast. Two 50 W UV light lamps (blue light lamps with an emitting wavelength of 385–400 nm) were used to stimulate the fluorescent dye. The excited fluorescent dye emitted red light with a wavelength in the visible range (635–700 nm). During the experiments, the ambient lights were turned off, and only the UV lights were used for illuminating the flow. Red filters were used on the cameras to further improve the visualization. Using fluorescent dye and UV light eliminated the reflections off the shiny surface of the inner pipes. Figure 2 shows a typical image obtained in our experiment (after removing the background image). The interface between the two fluids is clear, and the illumination is relatively uniform.

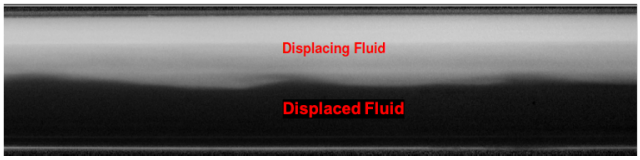

Figure 2. Example of an image showing both displacing and displaced fluids.

For imaging, two different cameras (Oryx 10 Gig model from FLIR industry with a 12 mm HP lens and f/1.8 and Prosilica GT 4096 camera from AlliedVision combined with a 50 mm Zeiss planar lens and f/1.4) were used. Measurements are carried out between 4.5 m and 6.0 m from the inlet (see the observation window in Figure 1). The data presented in this study were all recorded from 4.5-6.0 m away from the inlet (the measurement window in Figure 1). Camera 1 with a resolution of 2448 × 2048 and a frame rate up to 162 fps (frames/s) combined with a 12 mm lens was used for recording the full length of one pipe (1.5 m). Camera 1 provided roughly 1.7 pixels per mm of data (i.e., ≈ 85 pixels across the pipe outer diameter and 2448 along the axial length of the pipe). The second camera with a resolution of 4896 × 3264 and a 50 mm lens was used for zooming in over an approximately 40 cm length of the test section. Camera 2 provided 12.5 pixels per mm (i.e., ≈ 650 pixels across pipe diameter and 4896 over a 40 cm axial length).

2.3. Fluid Preparation and Rheological Properties

In our study, we focus in particular on simulating situations where the mud is difficult to remove, i.e., poor stand-off and significant mud yield stress. To simulate the yield stress property, we used an aqueous Carbopol polymer solution, as is often preferred over other viscoplastic fluids to be employed in flow visualization experiments [18,25,26]. Carbopol is highly transparent and relatively easy to prepare. Carbopol EZ-2 polymer from Lubrizol Inc. was used in our study. The mixing procedure for Carbopol was to mix a concentrated un-neutralized solution in 40 L of water overnight. The mixture was then neutralized in the tank using NaOH at a ratio of 1.0 g of NaOH to 3.5 g of Carbopol. The neutralized solution was then circulated through the system for 45 min to ensure homogeneity. The displacing fluids' rheology is shown in Figure 3a. This is most simply described by the Herschel–Bulkley model (Equation (1)).

$$\tau = \tau_y + \kappa \dot{\gamma}^n \quad (1)$$

where τ is the deviatoric stress (Pa), τ_y is the yield stress (Pa), $\dot{\gamma}$ is the shear rate (s^{-1}), κ is the consistency ($Pa \cdot s^n$), and n is the power law index. We can see that the fit to this model is reasonable. In general, we had a yield stress of 5–6 (Pa) for the displaced fluid.

In a cementing job, there is usually freedom in the design of the displacement process with respect to the spacer/wash. We aimed to study a range of displacing flow regimes. Thus, in addition to water, three solutions of xanthan gum (0.125%, 0.25%, and 0.5%) were used to simulate increasingly viscous spacers. The solutions of xanthan gum were shear-thinning (power law) fluids with some turbulent drag reduction properties [14], not usually very elastic at these concentrations; see Figure 3b. These displacing fluids were also mixed in concentrated batches overnight and diluted 45 min before experimenting. A high resolution Malvern Kinexus rheometer was used for rheological characterization of the test fluids, which was done immediately after the displacement experiments using experimental samples. The rheological properties are discussed below for each set of experiments.

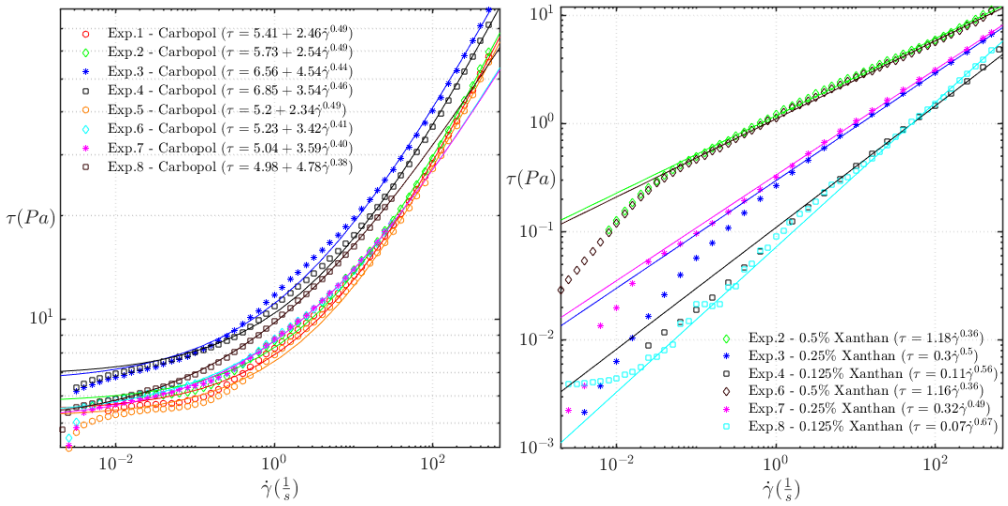

(**a**) (**b**)

Figure 3. Shear rheology data of (**a**) Carbopol and (**b**) xanthan (fitted model coefficients are reported in Table 2).

3. Results: Imposed Flow Rate Experiments

We first studied the impact on the displacement efficiency of changing the displacing fluid flow regime through manipulating the rheology. The displacing fluids had a similar imposed flow rate, but different concentrations of Xanthan gum were used to vary the flow regime. Two eccentricities were investigated (i.e., fully and 70% eccentric).

Both the displacing and displaced fluids had similar densities. A fixed Carbopol solution was displaced by both water and by different compositions of xanthan solutions (power law fluids). Rheological parameters were fit to the flow curve data and are reported in Table 2. All samples were pre-sheared in the rheometer before data acquisition.

Table 2. Rheological properties. of test fluids.

Experiment	e	Fluid Description	Fluid	τ_y (Pa)	κ (Pa·s^n)	n
1	1.0	Displacing	Water	–	1.002×10^{-3}	1
		Displaced	Carbopol (0.125%)	5.41	2.46	0.49
2	1.0	Displacing	Xanthan (0.5%)	–	1.18	0.36
		Displaced	Carbopol (0.125%)	5.73	2.54	0.49
3	1.0	Displacing	Xanthan (0.25%)	–	0.3	0.5
		Displaced	Carbopol (0.125%)	6.56	4.54	0.44
4	1.0	Displacing	Xanthan (0.125%)	–	0.11	0.56
		Displaced	Carbopol (0.125%)	6.85	3.54	0.46

Table 2. *Cont.*

Experiment	e	Fluid Description	Fluid	τ_y (Pa)	κ (Pa·s^n)	n
5	0.7	Displacing	Water	–	1.002×10^{-3}	1
		Displaced	Carbopol (0.125%)	5.2	2.34	0.49
6	0.7	Displacing	Xanthan (0.5%)	–	1.16	0.36
		Displaced	Carbopol (0.125%)	5.23	3.42	0.41
7	0.7	Displacing	Xanthan (0.25%)	–	0.32	0.49
		Displaced	Carbopol (0.125%)	5.04	3.59	0.40
8	0.7	Displacing	Xanthan (0.125%)	–	0.07	0.67
		Displaced	Carbopol (0.125%)	4.98	4.78	0.38

3.1. Scope of Experiments

The ranges of the flow conditions and measured average pressure drops for both displaced and displacing flows are summarized in Table 3. We studied fluid-fluid displacement flows under a constant nominal flow velocity (i.e., an imposed flow rate of ≈70 L/min). Note that Q_1 is the flow rate of the displaced fluid (Fluid 1, Carbopol) before switching the pneumatic valves and the displacing fluid enters the test section. At the flow rates imposed, these combinations of fluids represent a wide range of flow regimes, covering from a fully turbulent through transitional to high Reynolds number laminar flows. Here, we refer to the flow of the displacing fluid when discussing the regimes.

The recorded pressure drops for each test are reported in Figure 4. The sudden drop in the pressure marked the transition from displaced to displacing fluid in the experiments. The abrupt change in $\Delta P/\Delta L$ implies that a large portion of the displaced fluid in the annulus was removed quickly by the displacing fluid, resulting in the fast transition of the pressure drop from Fluid 1 (displaced fluid) to approximately that of Fluid 2 (displacing fluid). Furthermore, we note that the fluctuations in the registered pressure drops were more significant during the slower part of the displacement.

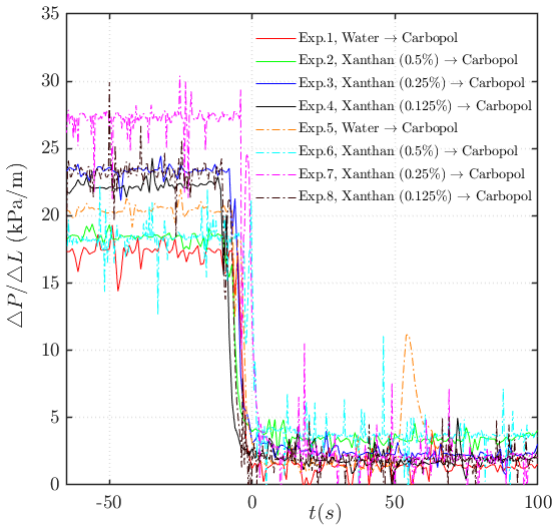

Figure 4. Recorded pressure drop profiles for each experiment—$\Delta P/\Delta L$ for both Fluids 1 and 2.

Additionally, the extent of the eccentric positioning of the casing pipe affected the annular pressure drop. The annular pressure drops for both fluids were lower in the experiments in the fully eccentric annulus, as is well known. As per the reported pressure drops in Table 3, the increase in the annular frictional pressure drop caused by the decrease in eccentricity from 1.0 to 0.7 was more pronounced for a yield-stress displaced fluid than for the Newtonian or power law displacing fluids.

Table 3. Flow rates (L/min) and pressure drops (kPa/m) associated with each experiment.

Experiment	e	Q_1 (L/min)	Q_2 (L/min)	$(\frac{\Delta P}{\Delta L})_1$ (kPa/m)	$(\frac{\Delta P}{\Delta L})_2$ (kPa/m)
1	1.0	69.3	74.4	17.3	1.4
2	1.0	71.1	72.1	18.5	3.8
3	1.0	68.7	71.0	23.4	2.5
4	1.0	72.2	73.5	22.3	1.9
5	0.7	70.9	70.8	20.5	1.6
6	0.7	72.8	73.4	18.2	4.3
7	0.7	71.4	70.1	27.3	2.4
8	0.7	72.0	75.5	23.3	2.1

3.2. Experimental Results at Full Eccentricity ($e = 1.0$)

Figure 5a,b shows the snapshots of the displacement process for Experiments 1 and 2, respectively. The black fluid is the Carbopol, and the time in each sequence of images is with respect to the first image in the sequence. Experiment 1 corresponds to a fully turbulent displacement (using water as the displacing fluid), while Experiment 2 corresponds to the lowest Reynolds number of displacing fluid (0.5% xanthan solution). Beyond $t = 30$ s, the displacement interface does not change appreciably with time. The distinction between the displacement mechanisms involved in laminar and turbulent displacements can be observed at the interface between the two fluids. The interface is relatively smooth at lower Reynolds numbers (Figure 5b) compared to that at higher Reynolds numbers (Figure 5a). In turbulent displacement, as shown in Figure 5a, the instantaneous streamwise shear-layer exhibits a wavy pattern between the non-turbulent and turbulent parts of the flow, contrary to the case in Figure 5b. This flow pattern might be caused by the large-scale flow structures that are typically found in turbulent plane Couette flow experiments [27] and simulations [28,29].

Regardless of the interfacial differences in laminar and turbulent shear-layers, all displacement scenarios investigated in this analysis are unsteady in the sense that the interface proceeds faster on the wide side and slower on the narrow side. This leads to the accumulation of highly viscous high yield stress Carbopol solutions on the narrow side. In an ideal displacement, one aims to avoid leaving mud behind, through either reducing the viscosity of the displaced fluid and enhancing turbulence or by increasing the viscoplastic stresses of the displacing fluid.

To compare the displacing candidates in Table 4 more precisely, it is customary in the literature to study the displacement quality using a non-dimensional displaced fluid height (i.e., h/D_o) or a volumetric efficiency $\eta(t)$, which is the percentage of mud that is displaced. Figure 6 schematically shows the concept of calculating different geometric factors required for the calculation of the volumetric efficiency of the displacement.

Table 4. Rheological properties of the test fluids.

Experiment	e	Fluid Description	Fluid	τ_y (Pa)	κ (Pa·s^n)	n
1	0.7	Displacing	Water	–	1.002×10^{-3}	1
		Displaced	Carbopol (0.125%)	5.21	3.46	0.40
2	0.7	Displacing	Xanthan (0.5%)	–	1.16	0.36
		Displaced	Carbopol (0.125%)	5.23	3.42	0.41
3	0.7	Displacing	Xanthan (0.25%)	–	0.28	0.49
		Displaced	Carbopol (0.125%)	5.25	3.77	0.39
4	0.7	Displacing	Xanthan (0.125%)	–	0.08	0.61
		Displaced	Carbopol (0.125%)	5.2	4.46	0.35

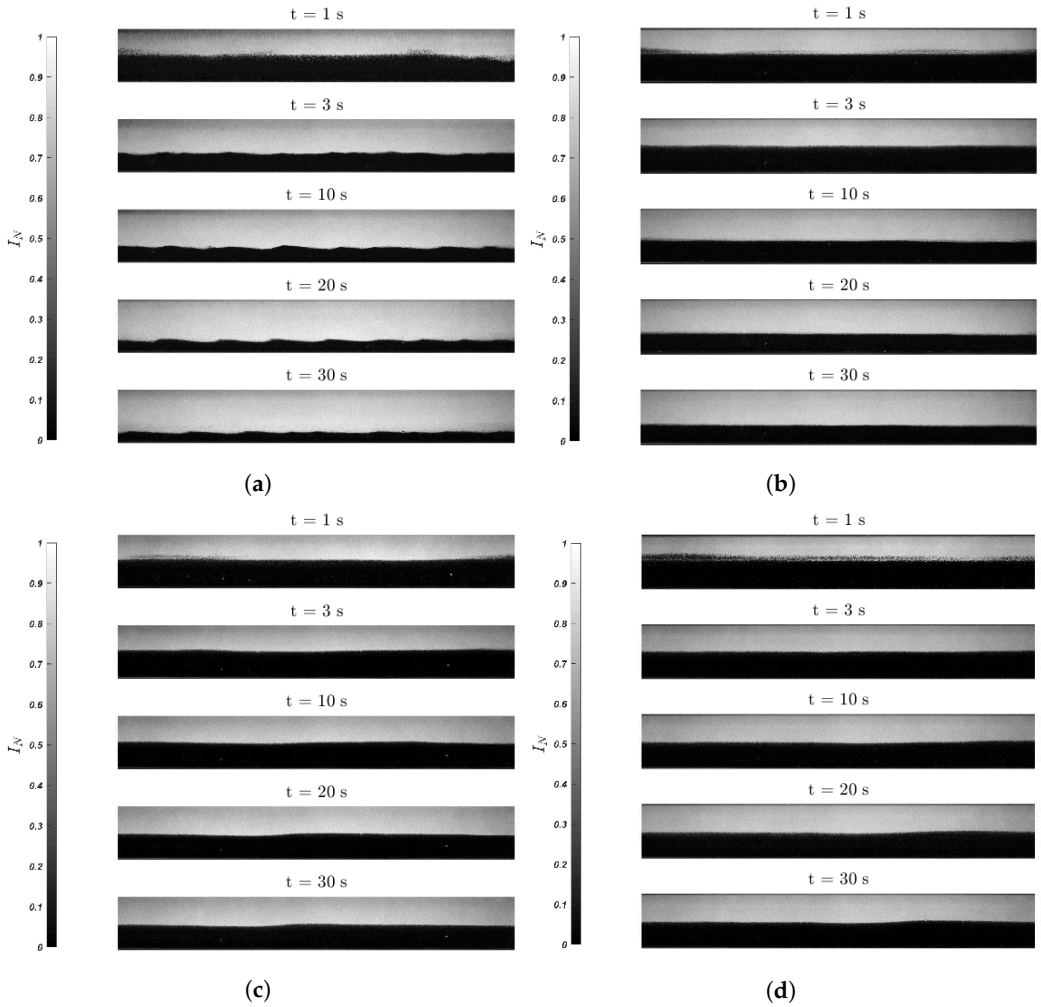

Figure 5. Displacement of Carbopol with (**a**) water in the turbulent regime (Experiment 1), (**b**) 0.5% xanthan solution in the laminar regime (Experiment 2), (**c**) 0.25% xanthan solution in the transitional regime (Experiment 3), and (**d**) 0.125% xanthan solution in the low Reynolds turbulent regime (Experiment 4), at full eccentricity.

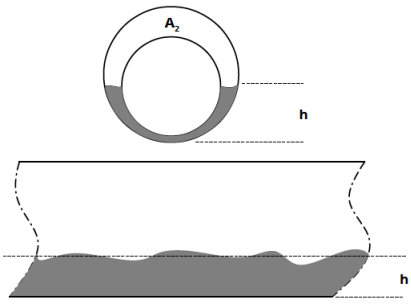

Figure 6. Schematic representation of calculating Carbopol layer thickness and volumetric efficiency.

At each instant through the experiment, the bulk velocity of Fluid 2 is computed using the following equation:

$$u_2 = \frac{Q_2}{A_2} \tag{2}$$

where Q_2 is the flow rate and A_2 denotes the cross-sectional area that is occupied by Fluid 2. Here, the flow cross-sectional areas are estimated using the average displaced fluid's

height estimated from the analysis of the snapshots of the displacement. The displacement efficiency is Equation (3):

$$\eta(t) = \frac{A_2(t)}{A} \tag{3}$$

Figure 7a shows changes in the non-dimensional displaced fluid heights (i.e., h/D_o), and Figure 7b compares estimated volumetric efficiency (η) over the displacement phase, respectively. The behavior of the non-dimensional displaced fluid height is an indicator of the efficiency of displacement in a concentric annulus, but in an eccentric annulus, the volumetric efficiency is underestimated: instead, h/D_o indicates the narrow side behavior of the annulus very well.

In terms of the thickness of the residual Carbopol layer (i.e., h), a height of about 25–55% of the Carbopol is not displaced. However, the estimated volumetric efficiency is in the range of 70–91%. The definition of displacement efficiency is deceptive, in that a 90% efficiency gives a biased impression of how effective a displacement has been. As we see, this is despite having significant displaced fluid left behind on the narrow side of the annulus. In practice, any residual mud channel allows for severe well leakage through gas invasion and leakage pathways that can also develop within the residual mud layers as they dry out [30,31].

The characteristics of the flow depend on the Reynolds number. Here, the Reynolds number (Re) is calculated using the generalized Reynolds number equation (Equation (4)) valid for power-law fluids [32] and is defined based on the fluid's mean bulk velocity (u_2) and its calculated hydraulic diameter ($D_{h,2}$):

$$Re = \frac{\rho {u_2}^{2-n} {D^n}_{h,2}}{K((3n+1)/(4n))^n 8^{n-1}} \tag{4}$$

$$D_{h,2} = \frac{4A_2}{P_{wet,2}} \tag{5}$$

where $P_{wet,2}$ is the wetted perimeter of the displacing fluid, including the interface. The results of the determination of the Reynolds number are shown in Figure 8. The range of the resultant Reynolds number experienced in each case varies due to changes in the mean flow velocity and hydraulic diameter. It can be observed that the flow regime is laminar for the displacement of Carbopol with the 0.5% xanthan solution (Experiment 2), while displacements of Carbopol with the 0.25% and 0.125% xanthan solutions (Experiments 3 and 4) are transitional and have low Reynolds turbulence, respectively. In the case of the displacement of Carbopol with water (Experiment 1), the displacing flow is fully turbulent. Despite the change in the flow regime from laminar and transitional in the case of Experiments 2–4 to turbulent in the case of Experiment 1, the displacement does not appear to be effective, as the Carbopol on the narrow side barely moves. Although the displacement is slightly improved in the case of Experiment 1, which appears to be due to achieving a highly turbulent regime, the displacement deteriorates in the case of Experiments 2 and 3 in comparison to Experiment 4, despite their weakly turbulent nature. The common understanding that a turbulent flow spreads around the annulus and delivers a more effective displacement is not found to be true in such fully eccentric annuli.

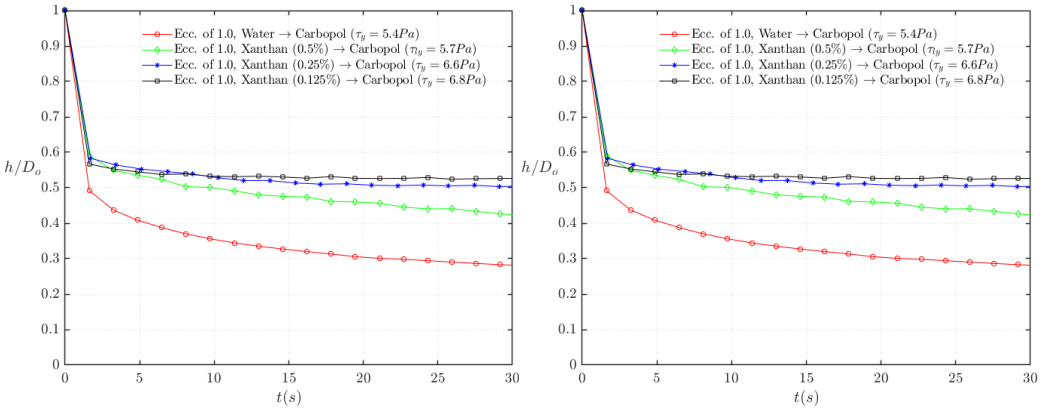

Figure 7. Displacement performance: (**a**) average measured thickness of the Carbopol layer in the fully eccentric annulus and (**b**) computed volumetric efficiency in the fully eccentric annulus.

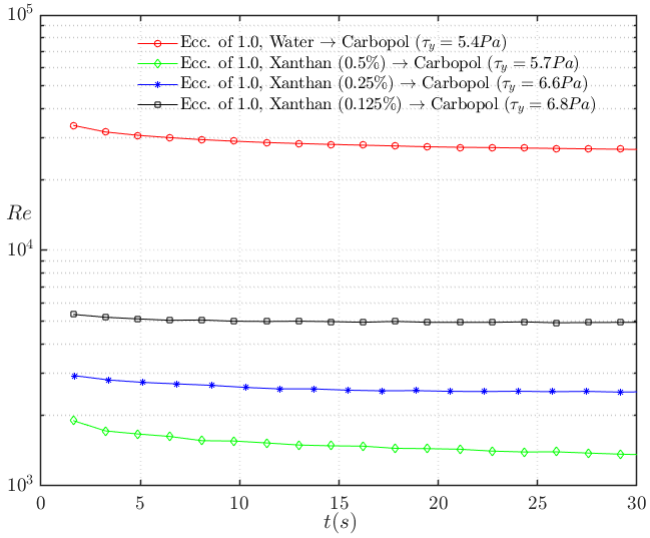

Figure 8. Computed Reynolds number for the displacing fluid in the fully eccentric annulus.

3.3. Experimental Results at Partial Eccentricity ($e = 0.7$)

In this series of experiments, the previous four experiments were repeated for an annulus with an eccentricity of 0.7. Figure 9a,b presents snapshots of the displacements of Carbopol by water (turbulent flow) and the 0.5% xanthan solution (laminar flow), respectively, at various times during the first 30 s immediately after switching the pneumatic valves. Similar to the previous cases, the turbulent displacement shows transient features such as ripples at the interface, while the interface remains flat in the case of the laminar displacement.

As shown in Figure 10a,b, as regards the non-dimensional displaced fluid heights (i.e., h/D_o) and volumetric efficiencies (η), we observed similar relative trends as in the first four experiments, but with an overall improvement in the efficiency of displacement and a reduction in the average height of the residual layer. We also see that similar to the displacements in the fully eccentric arrangement, a large portion of the Carbopol inside the annulus is displaced within the first few seconds. Through this initial displacement phase, the volumetric efficiencies of all experiments are within the same range regardless of the extent of eccentricity. However, the volumetric efficiency of the partially eccentric experiments eventually increases past those of the fully eccentric ones, indicating the facilitation of the removal of the static fluid from the narrow side of the annulus with a decrease in the degree of eccentricity.

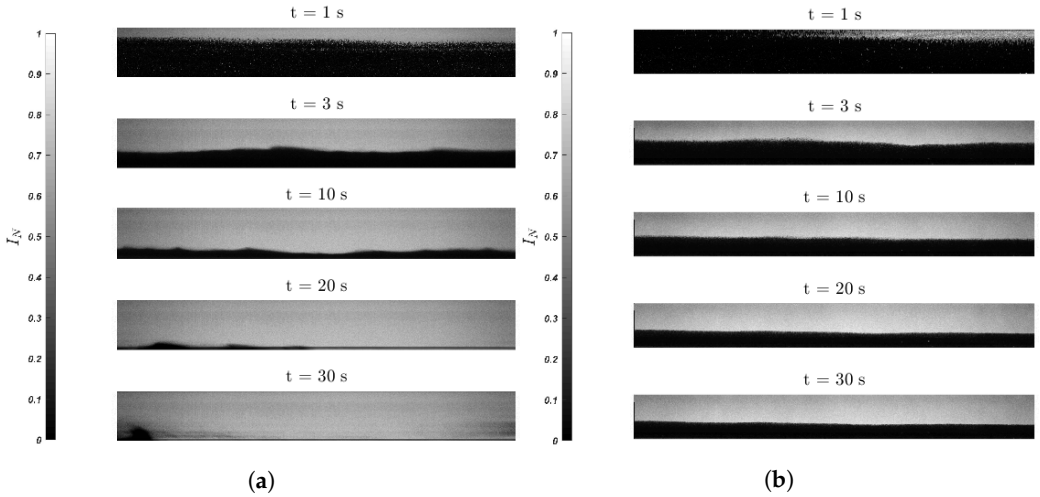

(**a**) (**b**)

Figure 9. Displacement of Carbopol with (**a**) water in the turbulent regime (Experiment 5) and (**b**) the xanthan solution in the laminar regime (Experiment 6), in a 70% eccentric arrangement.

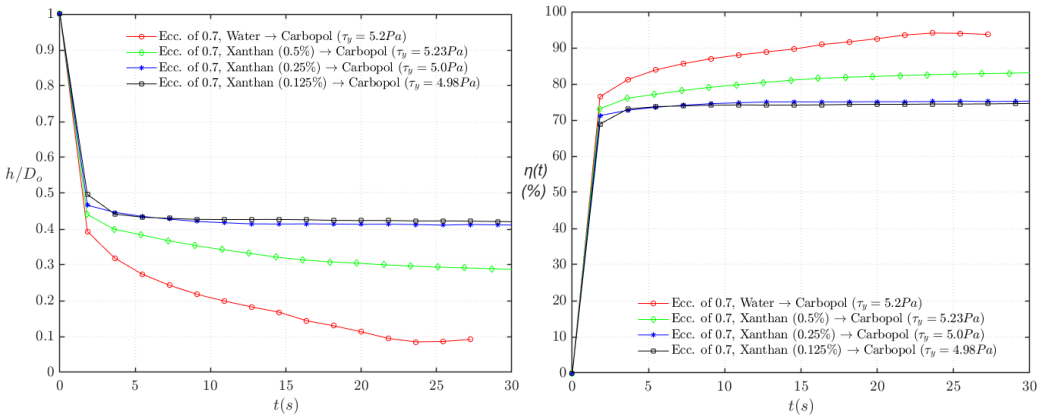

(**a**) (**b**)

Figure 10. Displacement performance: (**a**) Average measured thickness of the Carbopol layer in the partially eccentric annulus ($e = 0.7$) and (**b**) computed volumetric efficiency in the partially eccentric annulus ($e = 0.7$).

The computed Reynolds numbers for the experiments for the partially eccentric annulus shown in Figure 11 represent a wide range of flow parameters. We observe that the flow regime for the displacing fluid is turbulent in Experiment 5, transitioning to the weakly turbulent/transitional flow regime in Experiments 6 and 7 and the high Reynolds laminar regime in Experiment 8. Comparing Experiments 5–8 to 1–4, the displacement regimes remain relatively unchanged, and almost the same behavior is seen with respect to the effect of the flow regime on the displacement efficiencies. Turbulent displacement in the case of Experiment 5 is the most effective displacement scenario. However, comparing Experiments 6–8, the displacement deteriorates despite the transition from laminar displacement in Experiment 6 to higher Reynolds displacements in Experiments 7 and 8. As a result, it can be seen that even in an eccentric arrangement ($e = 0.7$), the highly viscous displacing fluid for laminar (or even high Reynolds laminar) displacement outperforms other less viscous transitional or low Reynolds turbulent displacements. Overall, despite the changes in the flow regime from turbulent to laminar and transitional, it appears that the displacement outcome is only marginally influenced by the displacement regime.

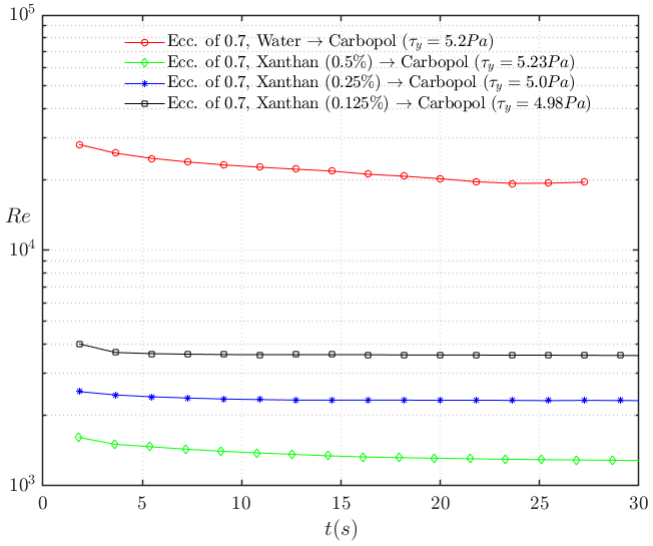

Figure 11. Computed Reynolds number for the displacing fluid in the partially eccentric annulus ($e = 0.7$).

In summary, the displacement efficiency is improved by the reduction of the eccentricity of the casing. According to some industrial guidelines, a maximum eccentricity of 25% to 33% (20% for cementing liners) should be maintained in order to achieve good quality cementing [1,33]. However, reducing eccentricity to this degree is challenging in horizontal and strongly deviated wells.

4. Results: Imposed Pressure Drop Experiments

In this set of experiments, in order to compare flow regimes and fluid designs under a typical field constraint, we kept the total frictional pressure drop generated by the displacing fluid over the length of the experimental setup constant. We again had no density difference between fluids. Different flow regimes (laminar to fully turbulent flow regimes) were investigated by changing the physical properties and flow rates of the test fluids.

The displaced fluid in these experiments was again Carbopol at a concentration of 0.125%. The mixing and rheological characterization procedures were as described earlier. Table 4 summarizes the displaced and displacing fluid pairs used in this set of experiments, as well as their fitted rheological parameters. The fluids used were similar to the experiments in the previous sections, but with the flow rate adjusted to match the target pressure drops for each displacing fluid.

4.1. Scope of Experiments

In this set of experiments, the flow rates were set for the different displacing fluids, to achieve almost the same frictional pressure of 4.3–4.5 kPa/m. Table 5 summarizes the flow conditions under which the displacement experiments were conducted and the measured average pressure drops for both fluids.

Table 5. Flow rates (L/min) and pressure drops (kPa/m) associated with each set of experiments.

Experiment	Q_1 (L/min)	Q_2 (L/min)	$(\frac{\Delta p}{\Delta l})_1$ (kPa/m)	$(\frac{\Delta P}{\Delta L})_2$ (kPa/m)
1	124.6	126.4	28.8	4.4
2	72.8	73.4	18.2	4.3
3	91.5	89.9	27.7	4.4
4	122.5	125.1	18.9	4.5

4.2. Experimental Results

Before analyzing various displacement scenarios and their associated efficiencies, we begin by presenting the displacement snapshots for Experiments 1 and 3 in Figure 12a,b, respectively. Experiments 1 and 3 represent turbulent and transitional displacements under constant pressure drop conditions along the annulus from $t = 1$ s to $t = 30$ s after the displacing fluid is introduced into the flow loop. Similar to previous cases with a constant flow rate, the transitional and high Reynolds laminar displacements exhibit a flat interface, while the turbulent case is characterized by a wavy interface. Both cases are unsteady displacements as the wide gap is displaced much faster than the narrow gap.

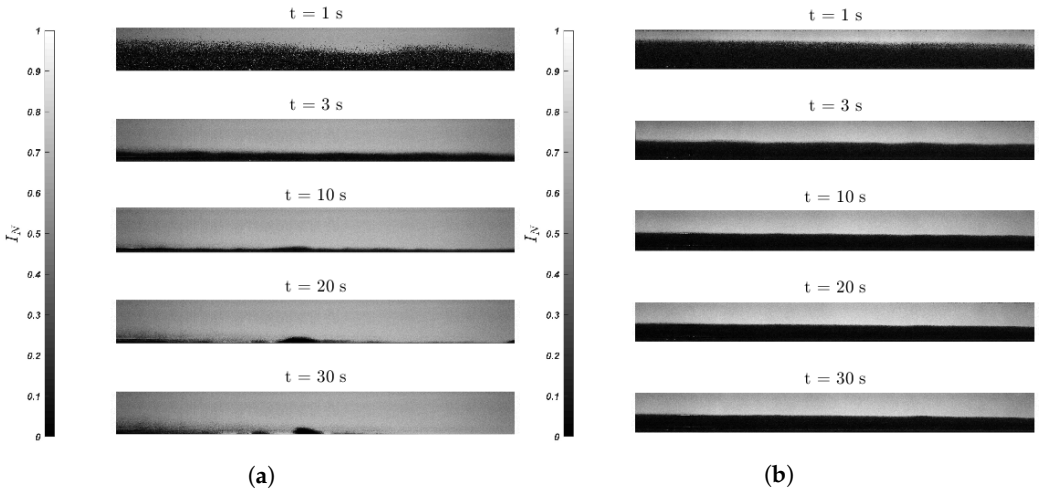

(**a**) (**b**)

Figure 12. Displacement of Carbopol with (**a**) water in the turbulent regime (Experiment 1) and (**b**) the xanthan solution in the transitional regime (Experiment 3) in an imposed pressure drop condition. See Figure 9b for Experiment 2 in this series.

Figure 13a plots the non-dimensional displaced fluid height (i.e., h/D_o) as a function of time (t), while Figure 13b presents the volumetric efficiency η during the displacement phase for all four displacing fluids. Despite the fact that the volumetric efficiency values are as high as 80–90%, none of the experiments can be considered fully successful. Indeed, the side views of the xanthan displacement in Figure 12b appear quite poor visually despite the reasonably high efficiency. This is purely an effect of the small volume on the narrow lower side of the annulus. The best volumetric efficiency is for water in Experiment 1 (fully turbulent), with the other three experiments with various xanthan solutions as the displacing fluid yielding almost the same results. This is interesting, because it appears that the laminar displacement (Experiment 2) performed almost equally as good as the low Reynolds turbulent displacements (Experiments 3 and 4). Although superior, using water in Experiment 1 still did not displace Carbopol fully from the narrow side during the recorded displacement phase of the experiment, and the efficiency grew only as high as 92% (see Figure 13b).

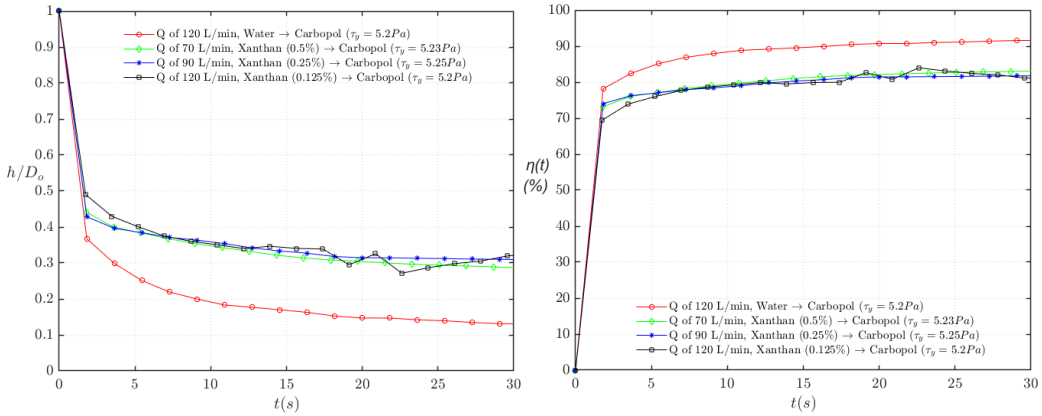

(**a**) (**b**)

Figure 13. Displacement performance: (**a**) Average measured thickness of the Carbopol layer in an imposed pressure drop condition and (**b**) computed volumetric efficiency in an imposed pressure drop condition.

The calculated Reynolds numbers for displacing fluid in all experiments are shown in Figure 14. We may regard the highest concentration of xanthan as being in a high *Re* laminar regime, while the other concentrations (Experiments 3 and 4) are transitional/weakly turbulent. In this context, it is interesting that there was little change in the results between the xanthan solutions. The fully turbulent water displacement showed an improvement in the volumetric efficiency, which we attributed to the enhancement of the velocity fluctuations and secondary flows.

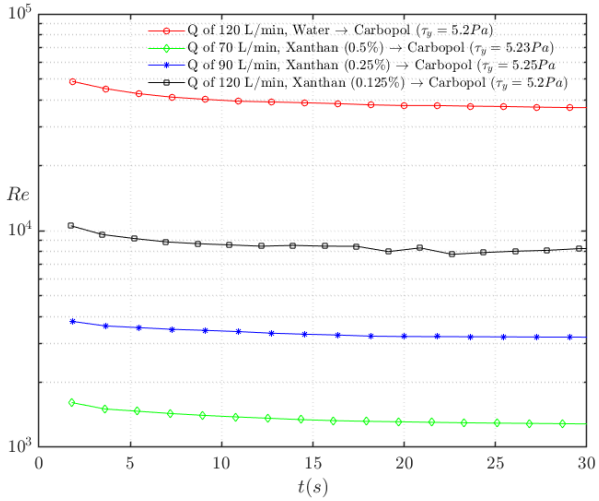

Figure 14. Computed Reynolds number for the displacing fluid in an imposed pressure drop condition.

5. Discussion

In this study, we performed a series of experiments that were aimed at simulating the performance of both Newtonian and non-Newtonian preflushes. Our objective was to study the role of the flow regime in regards to the displacement flows of yield stress fluids in eccentric horizontal annuli under both imposed flow rate and imposed pressure drop conditions.

In Section 3, we compared the effectiveness of different preflushes (i.e., water and various concentrations of xanthan solutions) at displacing the same Carbopol solution. A series of experiments was performed at a constant imposed flow rate (or pump capacity), achieving a range of flow regimes by the application of various displacing fluids. Our analysis suggested that the effect of the flow regime becomes very minimal in the range of weak turbulent and high Reynolds laminar flow regimes. The laminar displacement

flow marginally outperformed the weakly turbulent and transitional displacement flows. In Section 4, we imposed a constraint on the total frictional pressure drop, i.e., mimicking the field constraint of remaining within a required pressure range. These experiments also highlighted that the effect of the flow regime becomes insignificant in comparing laminar versus weakly turbulent displacement flows. However, the fully turbulent water produced the most efficient displacement.

We did not investigate the impact of buoyancy forces in this study. As shown by Maleki and Frigaard [15], buoyancy may be exploited to achieve steady displacement, while turbulence counters the effects of eccentricity. This is effective in vertical sections where buoyancy contributes to flow along the annulus. However, in a horizontal section, this effect is absent. Indeed, since washes are typically also less dense than the mud, buoyancy pushes washes towards the top of the annulus. This has been recently studied by Bizhani and Frigaard [16].

To summarize, if the goal is to achieve steady displacement along a strongly eccentric annulus filled with a yield stress fluid, the results suggest that this is very difficult. In all cases, there was a rapid breakthrough of the displacement front on the wide side, and we were left waiting considerably longer for the complete displacement to evolve. In our experiments at 70% eccentricity, the fully turbulent water produced more efficient displacements (larger η). However, this was still far from a steady displacement, and as shown in [16], including a density difference did not appear to effectively improve the displacement. Thus, the fully turbulent wash resulted in a displacement that was hard to control, as both rheology and buoyancy effects have been proven ineffective. In contrast, in laminar displacements, pumping much slower may allow time for both rheology and buoyancy to have an effect, and steady displacements can be found in horizontal displacement flows, e.g., see [34].

The other surprising aspect of our results was the insensitivity of our results in moving between high *Re* laminar to weakly turbulent regimes. Probably the high *Re* laminar flows are also not completely steady, and it may be that for all of these regimes, we have secondary flows of a similar (small) amplitude. It is interesting to note that as long as the industrial preference for turbulent flow cementing persists, it is likely that the more viscous fluids pumped in normal cementing operations will frequently flow in these ambiguous intermediate regimes.

6. Conclusions

We conclude that some of the simple statements/preferences widely employed in industry do not necessarily apply for all design scenarios. Instead, the detailed study of the fluids involved and specification of the operational constraints are needed to yield improved displacement quality in a consistent manner.

How to conduct such a study is less clear. Our study presents one set of example flows only. Thus, for example, for the eccentricity of 0.7, there is a slight benefit to using fully turbulent water, under either fixed flow rate or fixed pressure drop conditions, compared with the other fluids (weakly turbulent, transitional, or laminar). We cannot generalize such a statement without further study. This is a limitation of what we have done. Our work establishes the principle that one should study constrained flow designs in order to have industrial relevance. However, in the lab setting, we are limited to specific fluids for visualization. The answer is not necessarily a field setting (poor instrumentation) or even a large-scale yard test. As observed, effective turbulent displacements are very quick, and instrumenting a large-scale yard test adequately to capture these effects is prohibitively expensive.

Author Contributions: Y.F. and M.B. made equal contributions in the above publication, both in terms of performing the experiments, generating the content, and writing the drafts. I.A.F. supervised the project and assisted with writing the paper. All authors read and agreed to the published version of the manuscript.

Funding: Financial support for the study was provided by NSERC and Schlumberger through CRD Project No. 514472-17. The experimental infrastructure was funded by the Canada Foundation for Innovation and the BC Knowledge Development Fund, Grant No. CFI JELF 36069. This funding is gratefully acknowledged.

Institutional Review Board Statement: Not applicable.

Informed Consent Statement: Not applicable.

Data Availability Statement: The data presented in this study are available upon request from the corresponding author. The data are not publicly available due to the large volume of collected data.

Conflicts of Interest: The authors declare no conflict of interest.

References

1. Nelson, E. B.; Guillot, D. *Well Cementing*, 2nd ed.; Schlumberger: Sugar Land, TX, USA, 2006.
2. Lavrov, A.; Torsæter, M.; SpringerLink (Online service); SpringerLINK ebooks - Energy. *Physics and Mechanics of Primary Well Cementing*; Springer International Publishing: Berlin/Heidelberg, Germany, 2016.
3. Kelessidis, V. C.; Merlo, A.; Rafferty, R.; Borriello, G.; Guillot, D. J., Field data demonstrate improved mud removal techniques lead to successful cement jobs. *Soc. Pet. Eng. Adv. Technol. Ser. SPE-26982* **1996**, *4*, 53–58. [CrossRef]
4. Sauer, C.W. Mud displacement during cementing state of the art. *J. Pet. Technol.* **1987**, *39*, 1091–1101. [CrossRef]
5. Energy Safety Canada. *Primary Cementing: An Industry Recommended Practice (IRP) for the Canadian Oil and Gas Industry*; Drilling and Completion Committee: Calgary, AB, Canada, 2017.
6. Khalilova, P.; Koons, B.; Lawrence, D.; Elhancha, A. Newtonian Fluid in Cementing Operations in Deepwater Wells: Friend or Foe? In Proceedings of the SPE Annual Technical Conference and Exhibition, New Orleans, LA, USA, 30 September–2 October 2013; Society of Petroleum Engineering Paper Series, SPE-166456-MS; Society of Petroleum Engineering: Richardson, TX, USA, 2013.
7. Maleki, A.; Frigaard, I.A. Comparing laminar and turbulent primary cementing flows. *J. Pet. Sci. Eng.* **2019**, *177*, 808–821. [CrossRef]
8. Enayatpour, S.; Van Oort, E. Advanced Modelling of Cement Displacement Complexities. In Proceedings of the SPE/IADC Drilling Conference and Exhibition, The Hague, The Netherlands, 14–16 March 2017; Society of Petroleum Engineering Paper Series, SPE-184702-MS; Society of Petroleum Engineering: Richardson, TX, USA, 2017.
9. Smith, T.R.; Ravi, K.M. Investigation of Drilling Fluid Properties to Maximize Cement Displacement Efficiency. In Proceedings of the SPE Annual Technical Conference and Exhibition, Dallas, TX, USA, 6–9 October 1991; Society of Petroleum Engineering Paper Series, SPE-22775-MS; Society of Petroleum Engineering: Richardson, TX, USA, 1991.
10. Howard, G.C.; Clark, J.B. Factors to be considered in obtaining proper cementing of casing. *Drill. Prod. Pract. API* **1948**, *1948*, 257–272.
11. Haut, R.C.; Crook, R.J. Primary cementing: The mud displacement process. In Proceedings of the SPE Annual Technical Conference and Exhibition, Las Vegas, NV, USA, 23–26 September 1979; Society of Petroleum Engineering Paper Series, SPE-8253-MS; Society of Petroleum Engineering: Richardson, TX, USA, 1979.
12. Smith, T. R. Cementing displacement practices field applications. *J. Pet. Technol.* **1990**, *42*, 564–629. [CrossRef]
13. Brice, J.W.; Holmes, B.C. Engineered casing cementing programs using turbulent flow techniques. *J. Pet. Technol.* **1964**, *16*, 503–508. [CrossRef]
14. Guillot, D.; Desroches, J.; Frigaard, I.A. Are preflushes really contributing to mud displacement during primary cementing? In Proceedings of the SPE/IADC Drilling Conference, Amsterdam, The Netherlands, 20–22 February 2007; Society of Petroleum Engineering Paper Series, SPE-105903-MS; Society of Petroleum Engineering: Richardson, TX, USA, 2007.
15. Maleki, A.; Frigaard, I. A. Turbulent displacement flows in primary cementing of oil and gas wells. *Phys. Fluids* **2018**, *30*, 123101. [CrossRef]
16. Bizhani, M.; Foolad, Y.; Frigaard, I.A. Turbulent displacement flow of viscoplastic fluids in eccentric annulus: Experiments. *Phys. Fluids* **2020**, *32*, 045117. [CrossRef]
17. Maleki, A.; Frigaard, I.A. Using lightweight or low viscosity preflushes for primary cementing of surface casing. In Proceedigns of the 37th International Conference on Ocean, Offshore & Arctic Engineering, Madrid, Spain, 17–22 June 2018.
18. Maleki, A.; Frigaard, I.A. Primary cementing of oil and gas wells in turbulent and mixed regimes. *J. Eng. Math.* **2017**, *107*, 201–230. [CrossRef]
19. Nouri, J.M.; Umur, H.; Whitelaw, J.H. Flow of Newtonian and non-Newtonian fluids in concentric and eccentric annuli. *J. Fluid Mech.* **1993**, *84*, 617–641. [CrossRef]
20. Walton, I.C.; Bittleston, S.H. The axial flow of a Bingham plastic in a narrow eccentric annulus. *J. Fluid Mech.* **2006**, *222*, 39–60. [CrossRef]
21. Nikitin, N.; Yakhot, A. Direct numerical simulation of turbulent flow in elliptical ducts. *J. Fluid Mech.* **2005**, *532*, 141–164. [CrossRef]
22. Nikitin, N.; Wang, H.; Chernyshenko, S. Turbulent flow and heat transfer in eccentric annulus. *J. Fluid Mech.* **2009**, *638*, 95–116. [CrossRef]

23. Bizhani, M.; Frigaard, I.A. Buoyancy effects on turbulent displacement of viscoplastic fluids from strongly eccentric horizontal annuli. *Phys. Fluids* **2020**, *32*, 125112. [CrossRef]
24. Escudier, M.P.; Gouldson, I.W.; Jones, D.M. Flow of shear-thinning fluids in a concentric annulus. *Exp. Fluids* **1995**, *18*, 225–238. [CrossRef]
25. Gessner, F.B. The origin of secondary flow in turbulent flow along a corner. *J. Fluid Mech.* **2006**, *58*, 1–25. [CrossRef]
26. Dai, Y.J.; Xu, C.X. Wall pressure and secondary-flow origination in a square duct. *Phys. Fluids* **2019**, *31*.
27. Kitoh, O.; Nakabyashi, K.; Nishimura, F. Experimental study on mean velocity and turbulence characteristics of plane Couette flow: Low-Reynolds-number effects and large longitudinal vortical structure. *J. Fluid Mech.* **2005**, *539*, 199–227. [CrossRef]
28. Bech, K.H.; Tillmark, N.; Alfredsson, P.H.; Andersson, H.I. An investigation of turbulent plane Couette flow at low Reynolds numbers. *J. Fluid Mech.* **1995**, *286*, 291–325. [CrossRef]
29. Tsukahara, T.; Kawamura, H.; Shingai, K. DNS of turbulent Couette flow with emphasis on the large-scale structure in the core region. *J. Turbul.* **2006**, *7*, 1–16. [CrossRef]
30. Zare, M.; Roustaei, A.; Frigaard, I.A. Buoyancy effects on micro-annulus formation: Density stable displacement of Newtonian–Bingham fluids. *J. Non-Newton. Fluid Mech.* **2017**, *247*, 22–40. [CrossRef]
31. Vrålstad, T.; Skorpa, R. Digital cement integrity: A methodology for 3D visualization of cracks and microannuli in well cement. *Sustainability* **2020**, *12*, 4128. [CrossRef]
32. Madlener, K.; Frey, B.; Ciezki, H.C. Generalized Reynolds Number for Non-Newtonian Fluids. *EUCASS Proc. Ser.* **2009**, *1*, 237–250.
33. McPherson, S.A. Cementation of horizontal wellbores. In Proceedings of the SPE Annual Technical Conference and Exhibition, Dallas, TX, USA, 1–4 October 2000; Society of Petroleum Engineering Paper Series: Drilling Engineering, SPE-62893-MS; Society of Petroleum Engineering: Richardson, TX, USA, 2000.
34. Renteria, A.; Frigaard, I.A. Primary cementing of horizontal wells. Displacement flows in eccentric horizontal annuli. Part 1. Experiments. *J. Fluid Mech.* **2020**, *905*, A7. [CrossRef]